CrossMark

Seasonal prediction of Indian summer monsoon rainfall in NCEP CFSv2: forecast and predictability error

Samir Pokhrel[1] · Subodh Kumar Saha[1] · Ashish Dhakate[1] · Hasibur Rahman[2] ·
Hemantkumar S. Chaudhari[1] · Kiran Salunke[1] · Anupam Hazra[1] · K. Sujith[1] ·
D. R. Sikka[1]

Abstract A detailed analysis of sensitivity to the initial condition for the simulation of the Indian summer monsoon using retrospective forecast by the latest version of the Climate Forecast System version-2 (CFSv2) is carried out. This study primarily focuses on the tropical region of Indian and Pacific Ocean basin, with special emphasis on the Indian land region. The simulated seasonal mean and the inter-annual standard deviations of rainfall, upper and lower level atmospheric circulations and Sea Surface Temperature (SST) tend to be more skillful as the lead forecast time decreases (5 month lead to 0 month lead time i.e. L5–L0). In general spatial correlation (bias) increases (decreases) as forecast lead time decreases. This is further substantiated by their averaged value over the selected study regions over the Indian and Pacific Ocean basins. The tendency of increase (decrease) of model bias with increasing (decreasing) forecast lead time also indicates the dynamical drift of the model. Large scale lower level circulation (850 hPa) shows enhancement of anomalous westerlies (easterlies) over the tropical region of the Indian Ocean (Western Pacific Ocean), which indicates the enhancement of model error with the decrease in lead time. At the upper level circulation (200 hPa) biases in both tropical easterly jet and subtropical westerlies jet tend to decrease as the lead time decreases. Despite enhancement of the prediction skill, mean SST bias seems to be insensitive to the initialization. All these biases are significant and together they make CFSv2 vulnerable to seasonal uncertainties in all the lead times. Overall the zeroth lead (L0) seems to have the best skill, however, in case of Indian summer monsoon rainfall (ISMR), the 3 month lead forecast time (L3) has the maximum ISMR prediction skill. This is valid using different independent datasets, wherein these maximum skill scores are 0.64, 0.42 and 0.57 with respect to the Global Precipitation Climatology Project, CPC Merged Analysis of Precipitation and the India Meteorological Department precipitation dataset respectively for L3. Despite significant El-Niño Southern Oscillation (ENSO) spring predictability barrier at L3, the ISMR skill score is highest at L3. Further, large scale zonal wind shear (Webster–Yang index) and SST over Niño3.4 region is best at L1 and L0. This implies that predictability aspect of ISMR is controlled by factors other than ENSO and Indian Ocean Dipole. Also, the model error (forecast error) outruns the error acquired by the inadequacies in the initial conditions (predictability error). Thus model deficiency is having more serious consequences as compared to the initial condition error for the seasonal forecast. All the model parameters show the increase in the predictability error as the lead decreases over the equatorial eastern Pacific basin and peaks at L2, then it further decreases. The dynamical consistency of both the forecast and the predictability error among all the variables indicates that these biases are purely systematic in nature and improvement of the physical processes in the CFSv2 may enhance the overall predictability.

✉ Samir Pokhrel
 samir@tropmet.res.in

1 Indian Institute of Tropical Meteorology, Dr. Homi Bhabha Road, Pashan, Pune 411008, India

2 Indian National Centre for Ocean Information Services, Hyderabad, India

1 Introduction

Prediction of Indian summer monsoon rainfall (ISMR) requires a reliable modeling and forecasting skill since

long, due to its importance for the economy and the livelihood of the people of this region. It has a long legacy starting from the time of Blanford (1884), who associated ISMR with the snowfall over the Himalayas. During the era of Walker (1924) the role of Pacific Sea Surface Temperature (SST) came into the picture. The empirical models developed by the India Meteorological Department (IMD; e.g. Rajeevan et al. 2006a) based on several parameters (viz. pressure, temperature, wind, SST, etc.) was also unsuccessful to produce skillful seasonal monsoon rainfall prediction to the level of reliability (e.g. Gadgil et al. 2005). After the advent of the dynamical models, several Atmospheric General Circulation Models (AGCMs) were used to assess the ISMR prediction skill, but were not able to perform up to the satisfactory level (Sperber and Palmer 1996; Goswami 1998 etc.). Thereafter Coupled General Circulation Models (CGCMs) were used for ISMR forecast (e.g. Preethi et al. 2010; Krishnamurthy and Shukla 2011, 2012; Rajeevan and Nanjundiah 2009; Rajeevan et al. 2012; Pokhrel et al. 2013 and many more). Although CGCMs has a slight edge over the AGCMs (e.g. Chaudhari et al. 2013a), ISMR prediction skill is still very low despite all the efforts.

The basic premise of seasonal prediction is the existence of the slowly varying boundary conditions (Charney and Shukla 1981). Thus anomalous SST associated with basin wide event viz. El-Niño Southern Oscillation (ENSO), Indian Ocean Dipole (IOD) are found to be the primary source of predictability (Shukla and Wallace 1983; Brankovic et al. 1994; Kumar and Hoerling 1998). The predictable signal due to slowly varying boundary condition is, however constrained by the internal atmospheric dynamics (Intraseasonal oscillations; Goswami 1998; Ajaya Mohan and Goswami 2003; Goswami and Xavier 2003). It is known that potential seasonal predictability over the tropics is better as compared to the extra tropics (Shukla 1998; Phelps et al. 2004; Chen et al. 2010). It is due to the presence of large signal to noise ratio (SNR), which deteriorates in extra-tropics due to the presence of midlatitude synoptic-scale systems. In spite of large potential predictability in the tropics, predictability over Indian domain is very low (e.g. Kang et al. 2004; Kang and Shukla 2005; Wang et al. 2005). For AGCM, the predictability is the boundary value problem, however, in case of CGCM it is an initial value problem. So a thorough understanding of the impact of the different initial conditions in the Indian monsoon simulation by a CGCM is required.

The AGCM study of Phelps et al. (2004) has demonstrated that atmospheric initial conditions do not have great influence on seasonal mean predictability and the model forecast skill is mainly determined by the interannual variations in the SST anomalies. As per Reichler and Roads (2005) the influence of initial conditions on atmospheric variables last only for the first 3 weeks and for some, its

influence last up to 8 weeks. Chen et al. (2010) has shown (using model monthly mean temperature) that zeroth month lead time (L0) has the highest forecast skill and it decreases rapidly (slowly) over extra-tropics (tropics) with few exceptions. Over the tropical regions their model results show highest skill at L0 during summer monsoon season (JJA; June–August). They have attributed the predictability over tropics mainly to the anomalous SST and the role of atmospheric and land initial conditions is minimal. Slingo and Palmer (2011) argued that the decrease (increase) of model bias (skill) with the decreasing lead-time is also indicative of the dynamical model drift. In the context of ISMR, Singh et al. (2012) have studied the lead time dependency of predictability using two AGCMs and four CGCMs. They found higher predictability in the first month lead time (L1) and L0 for CGCMs and AGCMs respectively. They have speculated this difference to the higher spin-up time for CGCMs as compared to AGCMs. At times, however, estimates of predictability from the Atmospheric Model Intercomparision Project (AMIP) simulations have been questioned due to the absence of coupled air–sea interactions (van den Dool et al. 2006). Despite having proper representation of air–sea interactions, the systematic bias in the CGCM is the major hindrance to achieve the reliable seasonal predictability of ISMR (Turner et al. 2005; Chaudhari et al. 2013a). The systematic bias in CGCMs is not letting its skill to surpass that of AGCMs by sound margin, and the main causes behind the systematic bias are: improper representation of many basic physical processes (i.e. error in model physics) and error in initial conditions (i.e. some inadequacies in assimilation system).

Climate Forecast System version 2.0 (CFSv2; Saha et al. 2014a) of the National Centers for Environmental Prediction (NCEP) is a coupled atmosphere–ocean-land model, which is used for global forecast in different lead times (week to several months). CFSv2 shows considerable improvement in simulation of various aspects of the Indian summer monsoon (Saha et al. 2014b; Sahai et al. 2013) as compared to previous version (i.e. CFSv1; Pokhrel et al. 2012a; Chaudhari et al. 2013b), thus it is pertinent to check the sensitivity of prediction skill to the different initial conditions in the retrospective forecast of CFSv2. Previously Drbohlav and Krishnamurthy (2010; now onwards DK10) have done an extensive study to check thoroughly the forecast and predictability errors in CFSv1, which was constrained by the presence of various biases across the Indian ocean basin (Seo et al. 2007; Chaudhari et al. 2013b; Pokhrel et al. 2012a). Since there are many improvements in the simulation of Indian summer monsoon by its latest version CFSv2 (Saha et al. 2014b), it is expected that forecast and predictability errors might have different characteristics for different initial conditions, which may eventually sensitize the ISMR prediction skill.

This study focuses on the forecast and predictability errors at different lead times of CFSv2 hindcast simulations and elucidates importance of initial conditions and model physics for the prediction skill of ISMR. The initial conditions show a significant spread in atmospheric and oceanic state variables when they traverse through the peak of ENSO phase in the Pacific (during December, January and February month) to the presence of spring predictability barrier (during March and April month) and finally passes through the normal ENSO signal (during May month). Thus the skill of CFSv2 to simulate ISMR, initialized during these varied atmosphere and Ocean conditions is expected to have spread. This study tries to bring out those differences in terms of model and initial condition errors. Section 2 describes the model and hindcast runs, Sect. 3 describes the biases of various model parameters for different initial conditions. Section 4 discusses different monsoon metrics at different leads. Section 5 elaborates the spring predictability barrier aspect of the forecast and Sect. 6 explains the forecast and predictability errors and Sect. 7 summarizes and conclude the results.

2 Data and model

The CFSv2 retrospective forecasts are a set of 9-month long hindcasts initiated every 5th day starting from 1st January with four ensemble members per day for the period from 1982 to 2009. This 28-years ensemble retrospective forecast dataset from CFSv2 with 24 members is provided by NCEP (http://cfs.ncep.noaa.gov). Initial conditions for the atmosphere and ocean come from the NCEP Climate Forecast System Reanalysis (CFSR, Saha et al. 2010). Beginning at January 1st, 9-month hindcasts were initiated every 5 days with four cycles (00, 06, 12, 18 GMT) on those days. NCEP compiled the monthly estimates as follows: for each calendar month, the hindcasts with initial dates after the 7th of that month were used as the ensemble members of the next month. For example, the starting dates for the January ensemble members are (called as February release by NCEP) the January 11th, 16th, 21st, 26th, 31st, and the February 5th. For the analysis, we have utilized ensemble mean forecasts obtained by averaging of these 24 ensemble members.

CFSv2 (Saha et al. 2014a) used in retrospective forecasts consists of a spectral atmospheric model (GFS) at a high resolution of T126 (~0.937°) with 64 hybrid vertical levels and the advanced version of the GFDL Modular Ocean Model, version 4p0d (Griffies et al. 2004), which is a finite-difference model at 0.25–0.5° grid spacing with 40 vertical layers. The atmosphere and ocean models are coupled with no flux adjustment. The convection scheme employed in the atmospheric component of CFSv2 is the simplified

Arakawa–Schubert convection (Hong and Pan 1998), with cumulus momentum mixing and orographic gravity wave drag (Saha et al. 2010). It uses the rapid radiative transfer model (RRTM) shortwave radiation with advance cloud radiation integration scheme (Iacono et al. 2000; Clough et al. 2005; Saha et al. 2014a). It is also coupled to a four-layer Noah land-surface model (Ek et al. 2003) and a two-layer sea ice model (Wu et al. 1997; Winton 2000).

For validation of model simulations, we have used NCEP reanalysis dataset version-2 (NCEP-R2; Kanamitsu et al. 2002) for winds at 850 and 200 hPa. SSTs from Reynolds et al. (2002) and rainfall data (1979–2009) from Global Precipitation Climatology Project (GPCP; Adler et al. 2003) are used.

3 Simulation of mean and forecast error

This study uses Indian summer monsoon season (JJAS; June–September) data from 1982 to 2009 (i.e. for 28 years). The lead forecasts of January, February, March, April, May and June release (as termed by NCEP) are known hereafter as L5, L4, L3, L2, L1 and L0 respectively (This represents December, January, February, March, April and May initial conditions respectively). Accuracy in the simulation of mean climate is also linked with the forecast skill of a model (Delsole and Shukla 2010). Therefore, it is also important to know how well CFSv2 is able to mimic the mean state of the climate at different lead times.

3.1 Rainfall

The seasonal observed GPCP climatology of rainfall is marked by well known inter-tropical convergence zone (ITCZ) coinciding with the meteorological equator and its extension as South Pacific convergence zone (SPCZ) starting from the maritime continent (Fig. 1a). Typically Indian subcontinent is marked by continental and oceanic tropical convergence zone, the first being situated over the central India and the foothills of the Himalaya and the second over the equatorial Indian Ocean (Fig. 1a). It also shows the orographic high raining zones over Western Ghats and Myanmar coast along with the ocean basin of the Bay of Bengal and South China Sea, which is the breeding ground for the large number of synoptic scale systems (Goswami et al. 2003). The model simulated seasonal mean is shown for the L2 (i.e. March initial condition, Fig. 1h), just for a reference. The model simulations are realistic enough to get all the major raining bands. However, it overestimates (underestimates) over oceanic (land) regions, which is systematic in nature (Fig. 1i–n). The dry bias over land region and particularly over Indian region is a major concern, which is rather enhanced in CFSv2 as compared to its previous version (CFSv1; Saha et al. 2014b). In spite of these widespread biases, the grid-by-grid correlation with observation
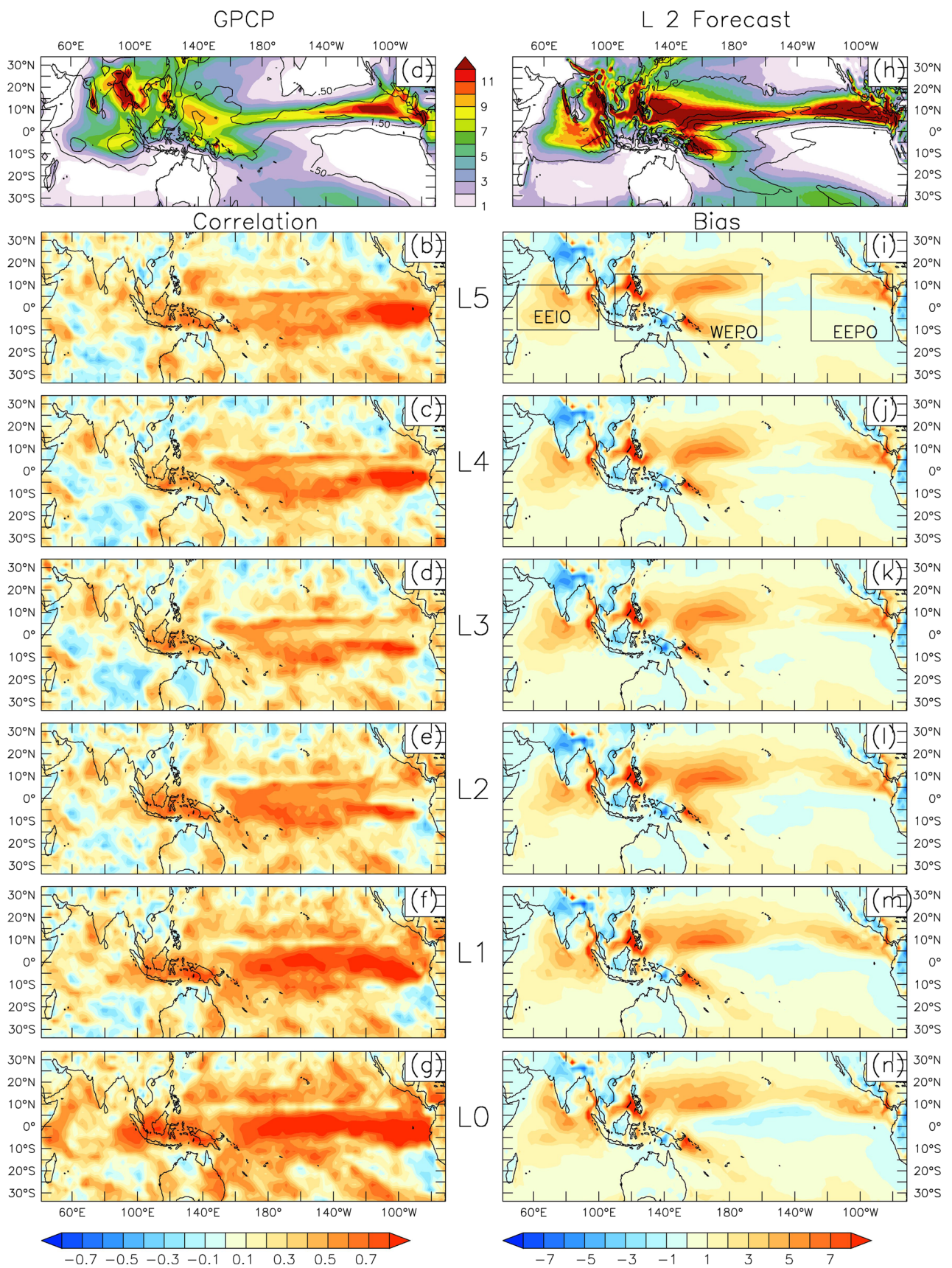
◄ **Fig. 1** JJAS mean rainfall (mm/day) in shaded and standard deviation in contour **a** GPCP and **h** CFSv2 (L2 Forecast). Spatial JJAS seasonal rainfall correlation between GPCP and CFSv2 for **b** L5, **c** L4, **d** L3, **e** L2, **f** L1, **g** L0 and bias for **i** L5, **j** L4, **k** L3, **l** L2, **m** L1 and **n** L0. The *boxes* in **i** represents the study regions for the estimation of quantitative values of model errors

becomes more robust with decreasing lead time of forecast (Fig. 1b–g). This indicates that overall rainfall tends to be more skillful at the last lead time (i.e. L0) over the Pacific and the Indian Ocean basin. This will be much clear by the quantitative values at some selected regions of interest. The rainfall biases, in general are pervasive and the nature of bias is almost constant in all the leads, this further confirms that biases are very systematic. Unlike correlation the amplitude of bias decreases marginally with decrease in forecast lead time.

The quantitative representation of biases in the mean and correlation coefficient is shown by Table 1, which is the averaged value over four regions closely linked with Indian summer monsoon. These four regions are East Equatorial Indian Ocean (EEIO; 50°E–100°E, 10°S–10°N), Western Equatorial Pacific Ocean (WEPO; 110°E–160°W, 15°S–15°N), Eastern Equatorial Pacific Ocean (EEPO; 130°W–80°W, 15°S–15°N) and the Indian land region (ILR). These regions are selected slightly extending Niño (related to El Niño) and IOD boxes over the Pacific and the Indian Ocean respectively, as they have the major influence on ISMR prediction. These regions are marked as boxes in Fig. 1i along with L5 rainfall bias. The dry rainfall bias over ILR decreases with the decreasing lead and attains least value of 1.2 mm/day at L0. The maximum correlation over ILR at L3 (0.21) also has the largest bias (−2.35 mm/day) and the same correlation value is also evident at L0. In case of oceanic regions, the correlation over EEIO (WEPO and EEPO) first decreases from L5 to L4 (L3) and then it increases to its maximum values at L0. The bias of both the regions over the Pacific basin (WEPO and EEPO) first increases till L3/L2 then decreases to its lowest value at L0, contrary to EEIO where rainfall bias first decreases

till L2 then increases to its maximum magnitude at L0 (see Table 1). Thus, except ILR the correlation (bias) in general attains least (largest) value during L3/L2, which symbolizes the well known aspect of the Spring Predictability Barrier (SPB), which will be discussed in Sect. 5.

Coupled model producing the reasonable facsimile of the observed interannual variability (IAV) has greater likelihood of better prediction (Sun and Wang 2013). Furthermore, a realistic simulation of IAV also depends upon the model's ability to simulate the mean accurately (Delsole and Shukla 2010). Thus, it is important to investigate the interannual variability of summer rainfall in CFSv2 with respect to observation. Since CFSv2 shows large systematic error in the mean rainfall, IAV of rainfall is also expected to be largely affected by these biases. Here IAV is represented as interannual standard deviation (SD) of the JJAS mean rainfall during different leads. Maxima of the interannual SD in observed rainfall (GPCP) in general coincides with regions of high rainfall, viz. over ITCZ, SPCZ and also over the eastern Indian Ocean, coastal Western Ghats, head Bay of Bengal and northeast India as shown by contour (Fig. 1a). Also, most of the oceanic high variability zones of rainfall converge with the high SST warm pool region (figure not shown). This establishes the fact that in the tropics, SST significantly controls the variability and hence the predictability of the rainfall.

Although CFSv2 is able to simulate the high SD zone over all the major raining bands, it does not coincide with the maxima of mean and rather there is a southward shift (particularly over ITCZ). Apart from this, CFSv2 overestimates (underestimates) the SD over the Pacific basin (eastern Indian Ocean and the Indian subcontinent; Fig. 1h). The magnitude and nature of this SD bias are maintained in all the forecast lead times, however, its amplitude slightly decreases (figure not shown). This underestimation of IAV of rainfall over land region is not unique to CFSv2 alone, almost all the models of the DEMETER project (Preethi et al. 2010) and that of the ENSEMBLES project (Rajeevan et al. 2012) too suffered from the similar problem. Rainfall

Table 1 Seasonal (JJAS) correlation and bias of CFSv2 rainfall with respect to GPCP over four different regions; (a) Indian land region (ILR), (b) East Equatorial Indian Ocean (EEIO; 50°E–100°E, 10°S–10°N), (c) Western Equatorial Pacific Ocean (WEPO; 110°E–160°W, 15°S–15°N) and (d) Eastern Equatorial Pacific Ocean (EEPO; 130°W–80°W, 15°S–15°N) at different leads

Rain	ILR		EEIO		WEPO		EEPO	
	Correlation	Bias	Correlation	Bias	Correlation	Bias	Correlation	Bias
L5	0.14	−2.32	0.18	2.47	0.34	2.09	0.45	1.24
L4	0.13	−2.27	0.06	2.46	0.34	2.15	0.41	1.27
L3	0.21	−2.35	0.08	2.45	0.30	2.22	0.30	1.30
L2	0.15	−2.18	0.15	2.30	0.38	2.27	0.32	1.18
L1	0.16	−1.65	0.22	2.41	0.44	2.07	0.49	1.12
L0	0.21	−1.20	0.36	2.57	0.51	1.84	0.56	1.11

over land is also governed by the robust coupling between slowly varying land surface state and atmospheric processes (Dirmeyer et al. 2006; Saha et al. 2011, 2012, 2013), which may be one of the probable components of these widespread biases over the land regions.

3.2 Winds at 850 hPa

The mean seasonal (JJAS) wind at 850 hPa is marked by intense south-westerlies over the north Indian Ocean, strong easterlies over tropical zone (20°S–20°N) of the Pacific basin and over the southern part of equator till 20°S in the Indian Ocean (Fig. 2a). CFSv2 has clearly simulated the mean features accurately with the differences being in the amplitude of the wind field (Fig. 2b). It is noteworthy that the equatorial easterlies are much more intense in CFSv2 and the maximum has a westward shift from the analysis field over the Pacific basin. As these easterlies over the equatorial Pacific basin form the lower branch of the planetary scale Walker circulation (Krishnamurti et al. 1973), this may have impact on ISMR predictability (e.g. Goswami et al. 1999; Soman and Slingo 1997; Pokhrel et al. 2012a). The south-westerlies (westerlies) over the north (equatorial) Indian Ocean are predominately underestimated (overestimated). The southern ocean westerlies (at 30°S) are also overestimated in the CFSv2.

The lead-wise bias clearly shows the error growth in the CFSv2 simulations (Fig. 2c–h). The south-westerlies over the north Indian Ocean is one of the most important aspects of the ISMR prediction, which is highly underestimated in L5 (Fig. 2c) and this underestimation decreases as the lead decreases (see Fig. 2h). This is expected as the target season is close to the initialization in L0 forecast as compared to the L5 forecast. The same holds true for the westerly jet at southern ocean (at 30°S). In this case overestimation reduces as the lead decreases. The most intriguing aspect seems to be the equatorial wind bias over both the Indian and the Pacific Ocean basins. Here the wind bias increases as the lead decreases. This zone lies over 2°S–8°N throughout the Indian Ocean basin, including maritime continent and also over the equatorial Pacific basin (10°S–10°N; 160°E–140°W). This is further clear by the quantitative values over the study regions as given in Table 2. The positive wind bias over EEIO (WEPO) increases as the lead decreases and attains largest value of 0.88 (0.68) m/s in L0. However, in case of EEPO, it decreases as the lead decreases and have its least value of 0.35 m/s at L0. Thus, combined regions of EEIO and WEPO together have opposite behaviors than EEPO. These equatorial regions play very important role in the equatorial wave dynamics through wind forcing, which is known to excite Rossby and Kelvin waves and helps in ocean heat adjustments through thermocline and mixed layer depth changes

(Schott et al. 2009). These biases, thus, play a significant role in defining SST variability and subsequent atmospheric response through the SST. These wind biases, thus, seem to hold the key for the ISMR predictability. Here one new aspect emerges, that all the biases do not decrease as the lead decreases, rather some biases increase as the lead decreases. Now it is important to know why the equatorial wind bias increases as the lead decreases, is it the initialization error or the model error. The error regarding model error and initialization error are discussed in Sect. 6.

3.3 Wind at 200 hPa

The upper level winds at 200 hPa is characterized by the tropical easterly jet (TEJ) over the Indian subcontinent region (centered around 10°N) and very intense upper level Southern hemispheric sub-tropical westerly jet (SSWJ) centered around 30°S (Fig. 3a). Strength of TEJ is related to the monsoon activity over the Indian subcontinent (e.g. Naidu et al. 2011). Strengthening (weakening) of TEJ is generally related to strong (relatively weak) monsoon over Indian region (e.g. Chaudhari et al. 2013b). SSWJ is an integral part of the tropical Hadley circulation, which is mainly driven by thermal forcing. Intense SSWJ in the model may lead to weak ISMR through relatively weak cross equatorial flow, as also seen in the previous version of the model (CFSv1; Chaudhari et al. 2013b). Tibetan high, as indicated by the upper level anticyclonic winds over the Himalayan region is also evident, which is basically maintained by the sensible heating at elevated terrain (Flohn 1968). Further, it may also reflect convective heating in the atmosphere forced by uplift of the air by the Himalayas (e.g. Yanai and Wu 2005). The location and intensity of Tibetan anticyclone are one of the important components of the monsoon circulation over Indian sub-continent. Since TEJ is located at the southern flank of Tibetan anticyclone, TEJ strength directly relates to a Tibetan anticyclone (e.g. Raghavan 1973; Krishnamurti and Bhalme 1976, etc.).

CFSv2 realistically simulates all the mean features (Fig. 3b), however, magnitude of TEJ is underestimated as compared to NCEP Reanalysis (Fig. 3a, b). Error in TEJ decreases with decreasing lead (starting from L5 to L0; Fig. 3c–h). CFSv2 is also able to replicate the position and strength of the Tibetan High (Fig. 3a, b). In case of SSWJ, its intensity is overestimated in CFSv2, however, there is a very marginal decrease in lead-wise SSWJ bias (Fig. 3c–h). Thus, model leads may have marginal impact on SSWJ. The quantitative value also justify the same (Table 3). Bias over all the study regions is least at L0, in case of EEIO and EEPO first it increases till L3, then it decreases to its least value in L0. The negative wind bias at L0 is 1.19, 0.83 and 0.61 m/s for EEIO, WEPO and EEPO regions respectively. Thus, there is a different behavior of the wind biases
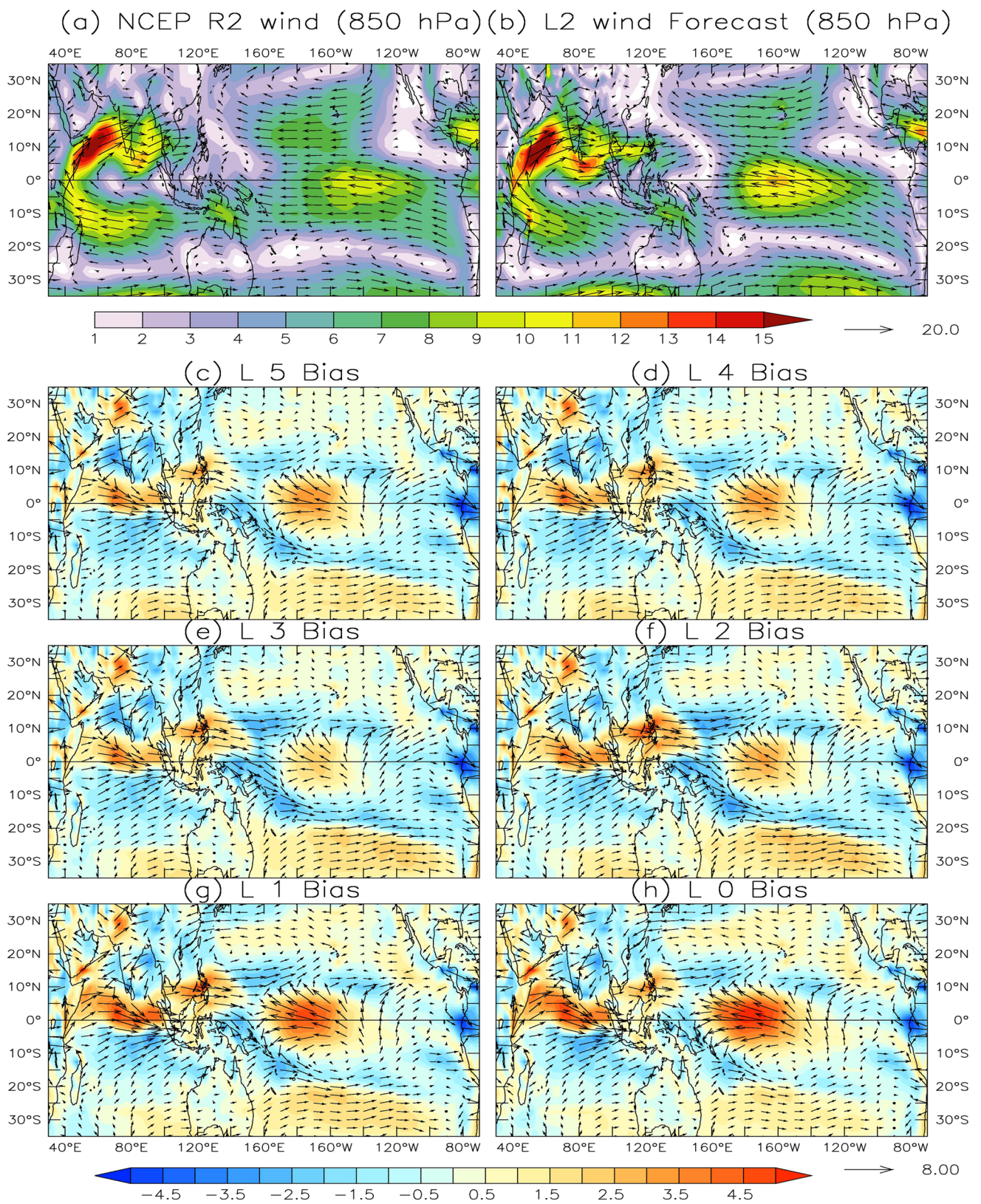
Fig. 2 JJAS mean wind speed at 850 hPa (m/s) in *shade* and direction as *vector* **a** NCEP Reanalysis-2 and **b** CFSv2 (Lead-2 Forecast). JJAS seasonal wind speed bias at 850 (*shaded*) and wind direction bias (*vector*) for **c** L5, **d** L4, **e** L3, **f** L2, **g** L1 and **h** L0

Table 2 Seasonal (JJAS) bias of CFSv2 winds at 850 hPa with respect to NCEP-R2 over the three oceanic study regions (EEIO, WEPO and EEPO) at different leads

Wind bias (850 hPa)	L5	L4	L3	L2	L1	L0
EEIO	0.24	0.32	0.32	0.58	0.86	0.88
WEPO	0.09	0.01	−0.24	−0.05	0.45	0.68
EEPO	−0.87	−0.88	−0.89	−0.65	−0.39	−0.35

at 850 and 200 hPa level over EEIO and WEPO regions. In the lower level (850 hPa) the wind bias increases with the decrease in lead and in the upper level (200 hPa) it shows the opposite to that of the lower level. However, in case of EEPO region wind bias at both levels decreases with the decrease in lead.

3.4 SST

SST is one of the most important parameters for the prediction of the ISMR (Saha 1970; Shukla 1975) as it controls the ocean response to the atmosphere in terms of various feedbacks. Warmer (colder) SST over the central and the eastern equatorial Pacific Ocean (i.e. ENSO events) has a tendency to substantially reduce (enhance) the amount of rainfall over the Indian subcontinent during monsoon season (Sikka 1980; Rasmusson and Carpenter 1983; Shukla 1987; Pokhrel et al. 2012a) through changes in planetary scale Walker circulation. Similarly the Indian Ocean SST too governs the ISMR through the modulation of regional Hadley circulation (Ashok et al. 2001) during IOD events. These SST variations are in general governed by subsurface ocean dynamics and surface heat flux forcing (Shinoda et al. 2004). The surface heat forcing is mainly controlled by the cloud cover.

Seasonal mean SST shows tropical warming due to constant solar insolation, and a warm pool region (SST > 28 °C) exist over the western Pacific Ocean and over the central and the eastern equatorial Indian Ocean basins (Fig. 4a). The prevalent tropical easterlies also tend to pile up equatorial warm waters over the western Pacific Ocean region. The inter-annual SD (overlaid contour) is maximum over the tropical central and east Pacific basins. The region with higher SD is also present over southern Bay of Bengal. As discussed above, the high variability of SST over eastern Pacific has a great impact on ISMR. Thus, any changes in the mean as well as SD values over these regions in different leads may have a influence on ISMR prediction.

CFSv2 realistically simulates all the general characteristic features of the observed mean SST (Fig. 4h). However the amplitude is considerably less which is evident by pervasive negative bias over the major part of the Pacific

and Indian Ocean basins in all the leads (Fig. 4i–n). In spite of having lower value of the mean, the SDs are quite high over the central and the eastern equatorial Pacific Ocean basins and also over some part of the central Indian Ocean basin (shown by contours in Fig. 4h). The spatial SST correlation between the observation and the model (shaded), increases as the lead decreases (Fig. 4b–g), which shows that SST simulations tend to be more realistic as the lead decreases, throughout the Indian and the Pacific basins. This is also clear by the presence of largest correlations over the study regions (Table 4) at L0 as compared to other leads (viz. 0.69, 0.71 and 0.75 in EEIO, WEPO and EEPO regions respectively). Even the bias in SD of SST over central, east equatorial Pacific basins and over the equatorial central Indian Ocean basin keeps on decreasing as the lead decreases (figure not shown). The SST bias seems to be invariant among all the leads, with pervasive cold bias throughout the study region, except the western coast of north and south America (Fig. 4i–n). In case of EEIO, the SST bias increases as the lead decreases till L1, thereafter it decreases to 0.76 °C in L0. In WEPO region, it decreases constantly as the lead decreases and attains least value of 0.27 °C at L0. Over EEPO, it shows no clear trend of increasing or decreasing SSTs.

The cold SST bias over north Indian Ocean is particularly due to the underestimation of near surface specific humidity, which eventually lead to higher evaporation and colder SSTs as also found in the freerun of CFSv2 (Pokhrel et al. 2012b). The warm (cold) bias over the eastern Pacific basin (rest of the region) is due to underestimation (over-estimation) of the low-level marine stratocumulus clouds (low and middle level stratus clouds; Yoo et al. 2013; figure not shown). Although some part of SST bias might be controlled by the ocean dynamics, these systematic biases in clouds, particularly over these regions, are dynamically consistent with the systematic biases in SST. The zonal surface wind in the model is stronger than the observation beyond L2 (figure not shown). Hence, apart from the radiative component (due to cloud cover bias) the turbulent heat flux in terms of latent heat may also play a major contributor for this large negative SST bias.
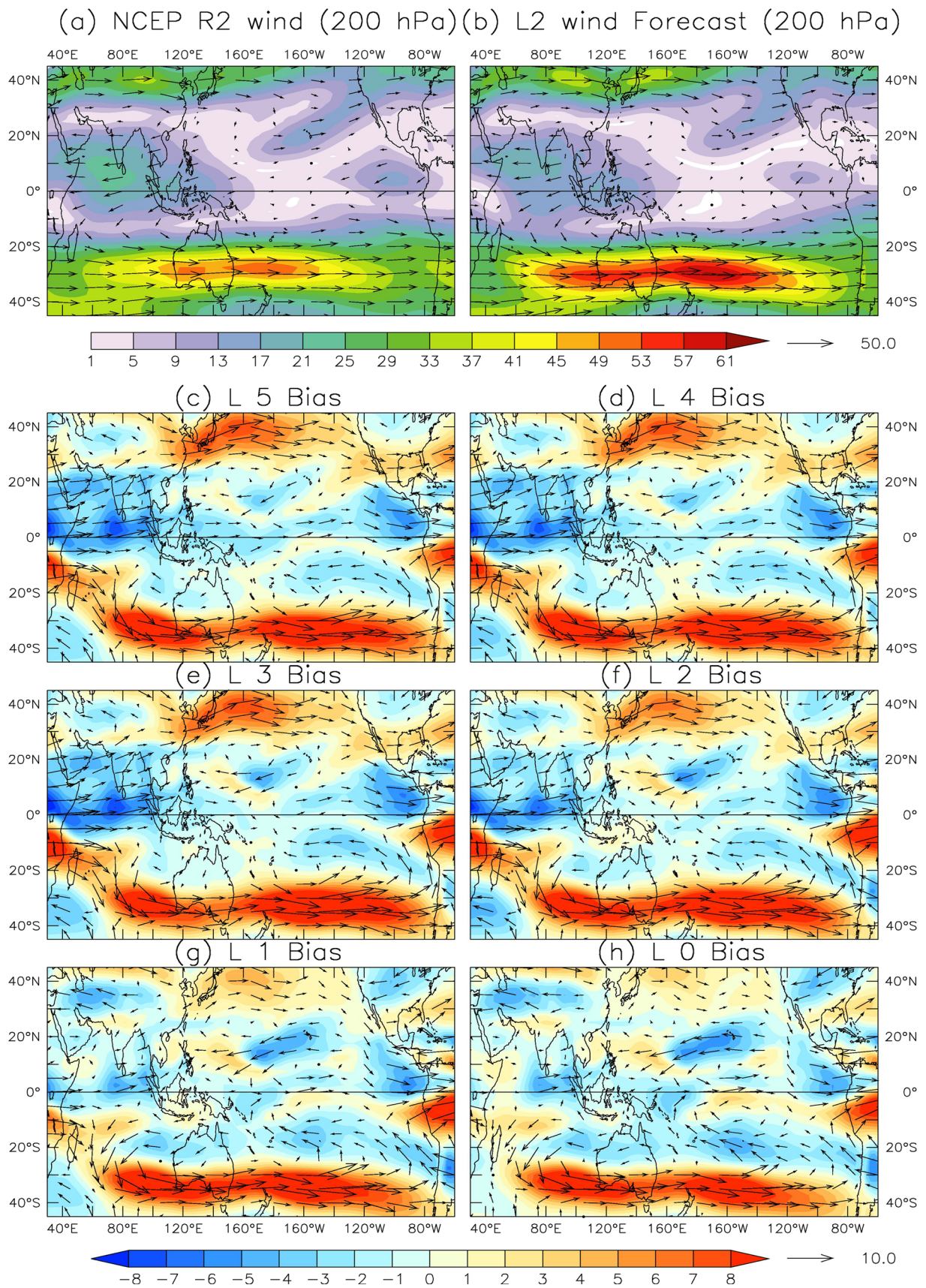
Fig. 3 Same as Fig. 2 but for wind at 200 hPa

Table 3 Same as Table 2, but for CFSv2 winds at 200 hPa

Wind bias (200 hPa)	L5	L4	L3	L2	L1	L0
EEIO	−3.69	−3.54	−4.01	−3.21	−1.68	−1.19
WEPO	−1.23	−1.01	−0.80	−0.41	−0.56	−0.83
EEPO	−1.91	−1.93	−2.06	−1.64	−0.86	−0.61

4 Indian summer monsoon indices

To assess the performance of the model quantitatively for the simulation of ISMR and its characterizing metrics in different leads, three very well known indices are used. Each of these three indices manifest different aspect of ISMR. The first being the ISMR index (Parthasarathy et al. 1995), which is the averaged rainfall over the Indian landmass, second one is Webster–Yang index (WY; Webster and Yang 1992), which represents the vertical shear of zonal wind between 800 and 200 hPa averaged over 0°N–20°N, 40°E–110°E and third being the Niño3.4 index, which is averaged SST values over Niño3.4 region (170°W–120°W, 5°S–5°N). The ISMR index is one of the most basic and widely used indices representing the overall monsoon performance. The WY index is a circulation index and describes the broad-scale South Asian monsoon variability that is primarily driven by convective heat sources. On the same line, Niño3.4 index represents the SST variability over the central equatorial Pacific basin and its proper simulation directly implies the possibility of better teleconnections through atmospheric response. Better representation of both WY and Niño3.4 indices may lead to better prediction of ISMR.

To compare the relative performance of these indices among different leads, Taylor diagram is used (Fig. 5a–c). Taylor diagram provides information of correlations, root-mean-square differences, and the ratio of variances (Taylor 2001). The distance from the origin is the normalized SD of the field with respect to the SD of the observed climatology. Also the distance from the reference point to the plotted point gives the root-mean-square difference (RMSE). Reference point represents the truth and is basically the position of the observed value with respect to other data to be compared. The correlation between the model and the observed climatology is the cosine of the polar angle. Thus the lead which has largest correlation, smaller RMSE and comparable variance will be close to the observations. Several studies have used Taylor plots for comparing model statistics (e.g. Pokhrel et al. 2013).

The skill score of ISMR in all the leads in terms of correlation has the range from 0.43 to 0.64 (also shown in Table 5) and the variance explained ranges from 55 to 75 % (Fig. 5a). L3 has the maximum correlation of 0.64 and explains 65 % of the observed variance. L1 too shares the equal variance as that of L3 and correlation

too is marginally less at 0.60. In terms of the best representation of variance, L2 performs the best, as it explains almost 75 % of the observed variance, but has a correlation of only 0.49. Thus, considering both correlation and variance together, L1 and L3 perform better for the ISMR skill score and among them, L3 is more robust. To check the consistency of maximum correlation at L3, we have also used IMD one degree gridded rainfall data (Rajeevan et al. 2006b) and CPC Merged Analysis of Precipitation (CMAP) data (Xie and Arkin 1997). Both these data sets show the same result (Table 5), wherein the largest correlation is at L3 (0.57 and 0.42), followed by L1 (0.51 and 0.34) for IMD rainfall and CMAP respectively.

In terms of circulation index (viz. WY index) performance, L1 performs the best, both in terms of correlation and variance, as it explains exactly the same variance as that of the reanalysis field and also has the largest correlation of 0.70 (Fig. 5b). L0 also performs better with the correlation of 0.67 and explains variance of 95 % of the reanalysis. L4 has the worst performance with a correlation of 0.28 and variance explained is 78 % of the reanalysis. L5 underestimates, however, L2 and L3 overestimate the variance. SST based index (viz. Niño3.4) skill is realistically captured by L0 and L1, with the correlation of 0.80 and 0.77 and variance explained is overestimated by 25 and 20 % respectively (Fig. 5c). Thus considering all the aspects of monsoon performance in terms of real precipitation skill score, circulation skill score and SST skill score, L1 has the best performance. However, in terms of ISMR prediction skill, L3 has best performance.

5 Spring predictability barrier (SPB)

The spring predictability barrier is known to be one of the factors responsible for the decrease in ENSO lead forecast skill during the spring season (Webster and Yang 1992; Duan and Wei 2013) and thus controls the ISMR skill. The rapid seasonal transition of monsoon circulation during spring time along with the existence of weak mean east–west SST gradient and very weak ocean–atmosphere coupling leads to spring predictability barrier (Webster and Yang 1992; Webster 1995). During the spring season the SST anomalies are relatively small in terms of predictable signal, which falls behind, in the presence of larger atmospheric and oceanic noises (Xue et al. 1994; Chen et al.
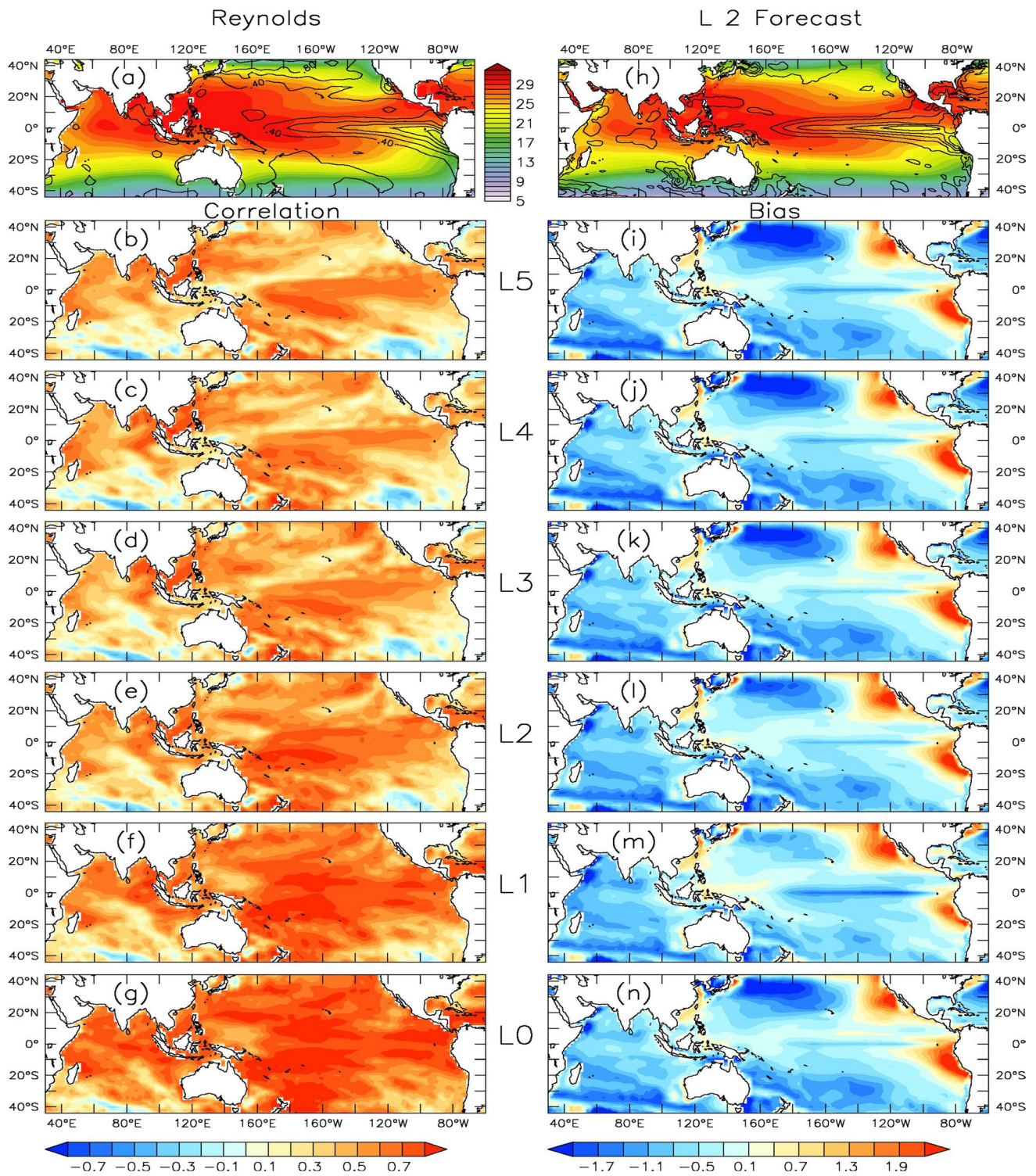
Fig. 4 Same as Fig. 1 but for SST. Here observational reference is Reynolds SST

1995). Thus, SPB is basically intrinsic physical property of ENSO forecasting (Samelson and Tziperman 2001) and consequently it reflects back into ISMR forecasting. CFSv2 is able to realistically simulate the presence of SPB in both Niño 3.4 and IOD indices (particularly at L3), indicating its robustness in ENSO forecasting (figure not shown). Despite the presence of SPB in ENSO and IOD signals, ISMR prediction skill is maximum at L3, thus there may be some phenomena other than ENSO and IOD which may control the ISMR prediction in CFSv2.

Table 4 Same as Table 1, but for CFSv2 SST's

SST	EEIO		WEPO		EEPO	
	Correlation	Bias	Correlation	Bias	Correlation	Bias
L5	0.48	−0.66	0.45	−0.41	0.51	0.24
L4	0.49	−0.70	0.47	−0.40	0.46	0.30
L3	0.43	−0.72	0.51	−0.38	0.48	0.40
L2	0.48	−0.85	0.60	−0.32	0.56	0.21
L1	0.59	−0.89	0.67	−0.28	0.69	−0.16
L0	0.69	−0.76	0.71	−0.27	0.75	−0.31
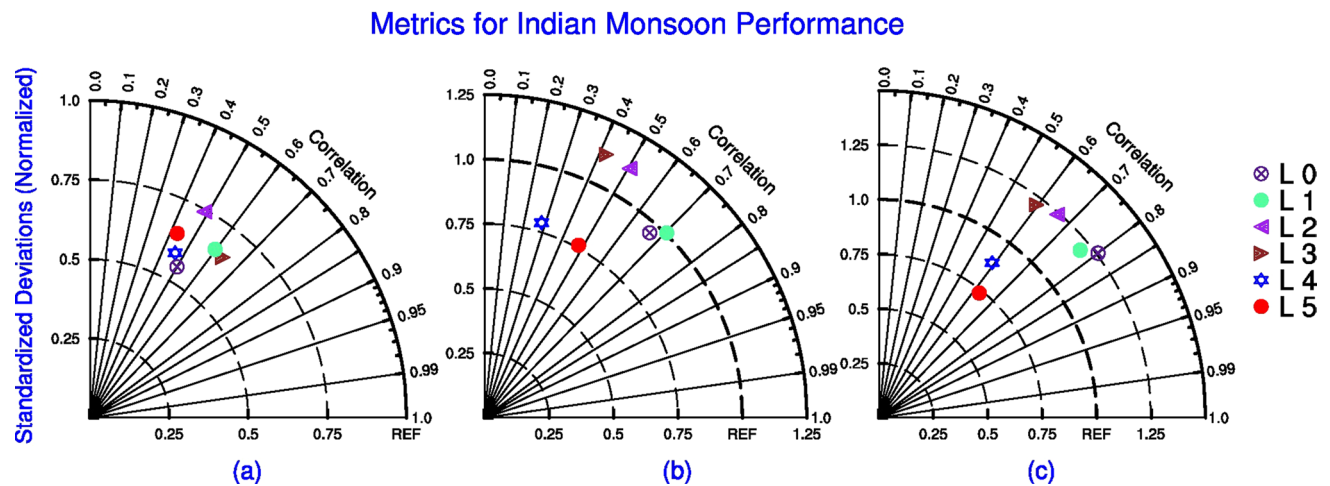
Fig. 5 Taylor plot for all the leads of the CFSv2 for **a** ISMR, **b** WY index and **c** Niño3.4 index

Table 5 Skill of ISMR with respect to three independent data, viz. GPCP, CMAP and IMD

ISMR skill (with respect to)	L5	L4	L3	L2	L1	L0
GPCP	0.43	0.46	**0.64**	0.49	0.60	0.50
CMAP	0.15	0.23	**0.42**	0.12	0.34	0.23
IMD	0.26	0.37	**0.57**	0.33	0.51	0.36

All the skill scores are calculated for the base period of 1982–2009 (28 years). The correlation coefficients (shown in bold) represent the maximum skill scores at L3 from all the independent data sets, which are significant at 99 % confidence level, except CMAP correlation skill, which is significant at 98 % confidence level

5.1 Cross correlation

The cross correlation of both ENSO and IOD indices with ISMR is shown in (Fig. 6a–c). First two panels of Fig. 6a, b represents cross-correlation for CFS simulations for all the start times and all the lead months (e.g. first column of the Fig. 6a shows correlation of 1st, 2nd, 3rd, …, 10th month's Niño 3.4 index with ISMR (rainfall during JJAS) of L5 simulations from bottom to top respectively, and the second column represents the similar correlation for L4 and so on till L0) and the third panel (Fig. 6c) shows the observed correlations. In case of observation, we get single value of correlation of ISMR for each month's Niño 3.4 index, which is therefore shown as a line plot, with the abscissa (ordinate) representing months of a year (correlation).

CFSv2 simulated Niño 3.4 index shows statistically significant negative correlation with the ISMR in JJAS season for all the initial conditions, which is similar to the observations. In case of IOD index, although the observed values are positive and significant during the July month (Fig. 6c), CFSv2 is completely out of phase with the observed ones (as the correlations are negative, instead of positive; Fig. 6b). This further testifies that CFSv2 is unable to depict the actual relationship between IOD index and ISMR. It may be due to very strong ENSO signal in the model (as indicated by the significant negative cross
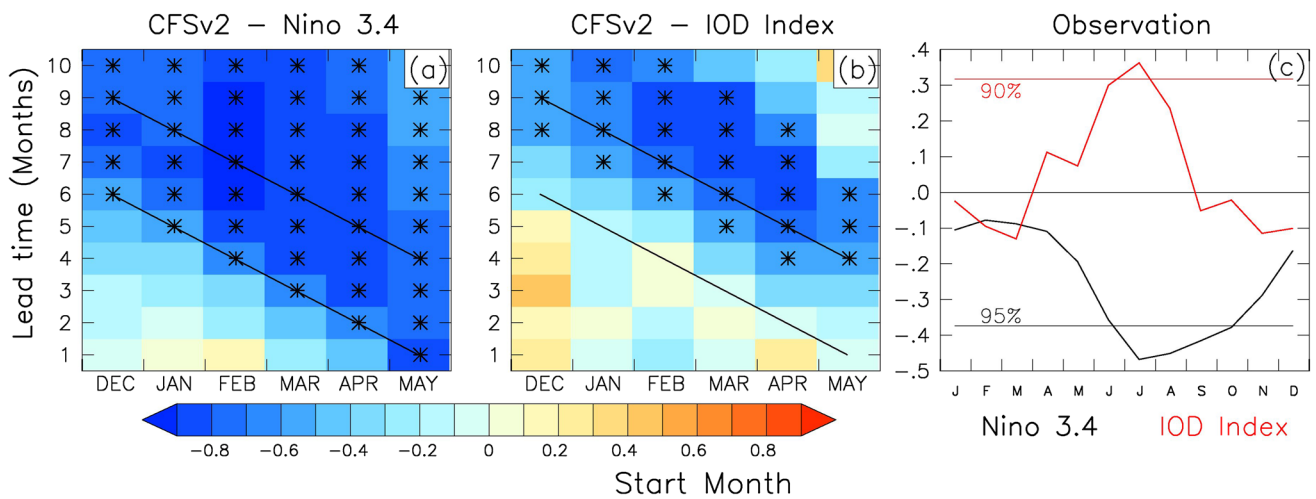
Fig. 6 Cross correlation as a function of start time and lead months between CFSv2 simulated ISMR and **a** CFSv2 simulated JJAS averaged Niño3.4 SST and **b** CFSv2 simulated IOD index. The area between two *slanting lines* represents JJAS season. The same cross correlation (**c**) between GPCP ISMR and Reynolds Niño3.4 index and IOD index. The correlation significant at 99 % confidence level is marked by *asterisk symbol*
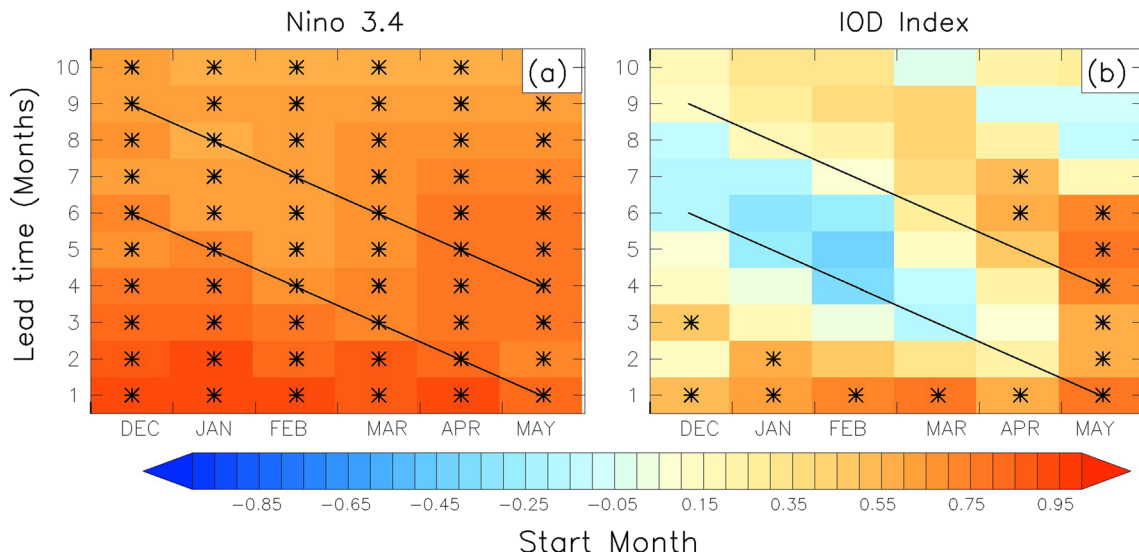

Fig. 7 Skill as a function of start time and lead months between observed values and CFSv2 simulations for **a** Niño3.4 index and **b** IOD index. The area between two *slanting lines* represents JJAS season. The correlation significant at 99 % confidence level is marked by *asterisk symbol*

correlation) which dominates the model simulated weak IOD signal. Thus, it is not viable to study the skill in a combined way, rather we have to see explicitly pure ENSO signal (i.e. ENSO without concurring IOD) and pure IOD signal (i.e. IOD without concurring ENSO).

5.2 Skill

The simultaneous correlation of model simulated and observed values for both Niño 3.4 and IOD indices clearly establish that prediction of ENSO is skillful in CFSv2 (Fig. 7a, b). All lead months of all start times are significantly correlated with the observed Niño 3.4 index. This indicates that for the ENSO prediction, the start time becomes immaterial. However, this is not true in case of the IOD index. In case of IOD index, the hindcast skill is significant till 1 month lead time for December to April initialization. However, for May initial conditions its IOD prediction skill remains significant till 6-month lead time. Despite, both ENSO and IOD has the best skill at May start time (i.e. L0), ISMR skill is highest at L3. This indicates the role of processes other than ENSO and IOD to be involved in dictating ISMR skill at L3 in CFSv2 simulations.
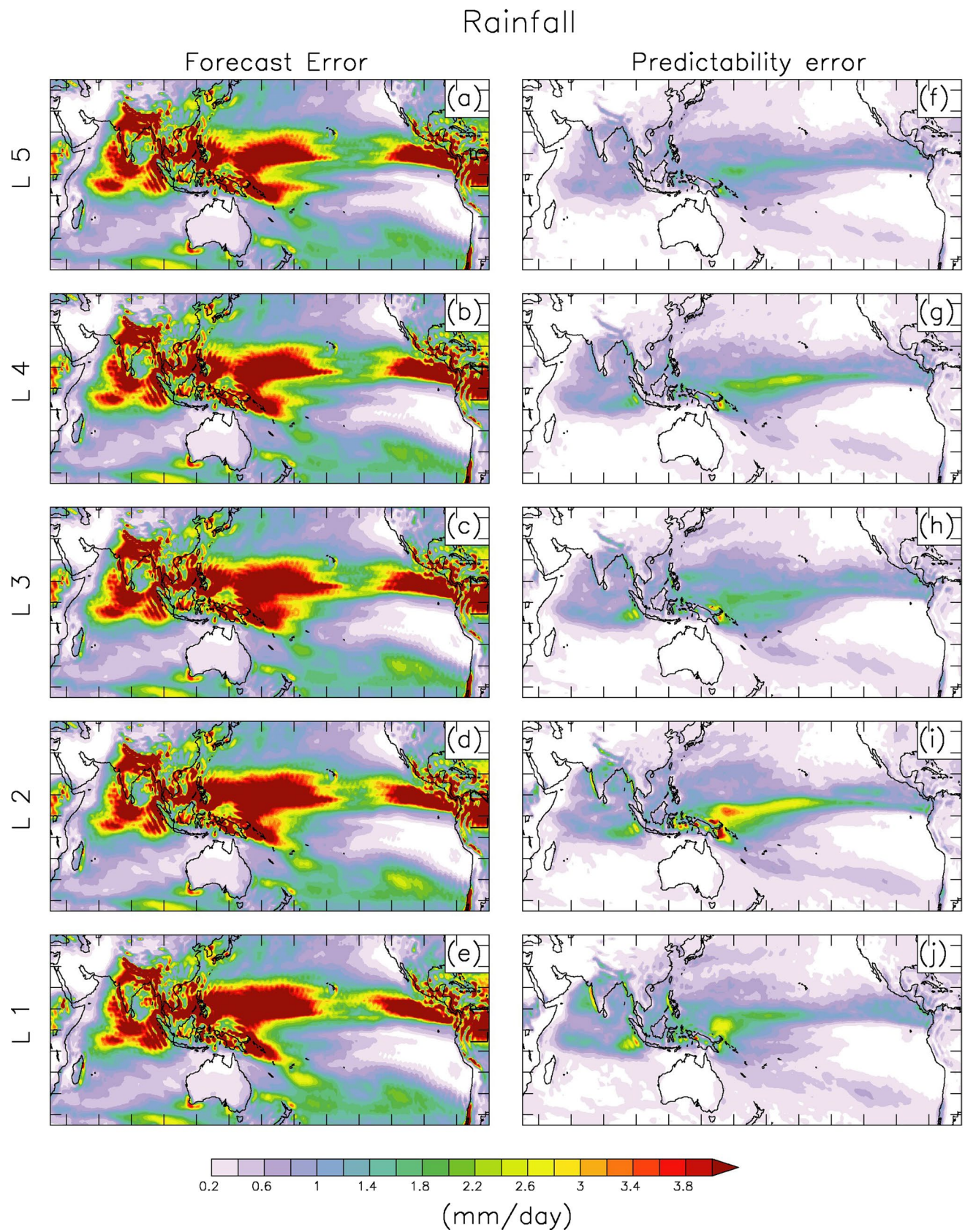
Rainfall

Fig. 8 Forecast error of rainfall at **a** L5, **b** L4, **c** L3, **d** L2, **e** L1 and Predictability error of rainfall at **f** L5, **g** L4, **h** L3, **i** L2 and **j** L1

6 Forecast and predictability errors

The predictability of a model is characterized by two types of errors. One being the model error, i.e. errors arising due to imperfection in the model due to its parameterization schemes, resolution, truncation, ill representation of physical processes etc. and other being due to the initialization (DK10). Forecast error is the deviation of the model results with respect to the observations (which has been discussed so far), which represents error due to all possible reasons (i.e. model physics, dynamics, initial conditions etc.). The predictability error arises due to error in the initial condition, assuming the model to be perfect (DK10). The sensitivity of predictions on initialization may be better represented by the predictability error as compared to forecast error. The predictability error is represented here as the deviation between the model's two lead forecasts at 1 month apart (i.e. L5 predictability error = L5 − L4 etc.). Now to get these deviations in absolute term, we find the RMSE and calculate the final forecast or predictability error. Suppose $X_{i,j}$ is the prediction of a variable corresponding to ith season (i = 1982–2009) of the jth lead time in month (j = 5, 4, 3, 2, 1) for "N" number of years and O_i is its analogous observed values, then forecast error (FE) and predictability error (PE) corresponding to the jth lead time will be

$$FE_j = \sqrt{\frac{\sum_{i=1}^{N-1}(X_{i,j} - O_i)^2}{N}} \qquad (1)$$

$$PE_j = \sqrt{\frac{\sum_{i=1}^{N-1}(X_{i,j} - X_{i,j-1})^2}{N}} \qquad (2)$$

A Similar approach was utilized by various previous researchers as well (e.g. DK10). Here we have identified those regions, wherein the effect of initialization may lead to significant model error in case of monsoon seasonal forecast. Even with a perfect model, a small error in the initial conditions (which is unavoidable) can spoil the predictability. Furthermore, a prediction from dynamical system

may be more accurate because of a particular set of initial conditions (e.g. Kleeman 2002).

6.1 Rainfall

In any non-linear system, the initial error grows with time may make the system unpredictable (Lorenz 1963). This is clearly seen as the model forecast error has much higher value as compared to the predictability error for the same lead. This implies that model errors are the major ones and the initial condition errors are of secondary importance (Fig. 8a–j). All the major raining band, including the ITCZ, SPCZ, both the convergence zone corresponding to the Indian monsoon (viz. continental and oceanic tropical convergence zone) and also Western Ghats of India have significant forecast error at all the leads (Fig. 8a–e). This indicates that the cumulus parameterization and grid-scale cloud microphysics schemes used in the model may induce errors in the rainfall simulations. This may be further augmented by the errors in the prediction of large scale circulation features and forecast fields which influences it (viz. SST) by providing erroneous ingredients for these parameterization schemes.

Predictability error is more concentrated over the equatorial belt of the western Pacific and the eastern Indian Ocean basins (Fig. 8f–j). Overall the predictability error decreases as the lead increases. This represents the ability of the model to reach at two different states which is very close to each other, if initialized with sufficient longer leads. This may be due to the long term inertia effect of slowly varying boundary conditions, which is the basic premise of seasonal prediction (Charney and Shukla 1981). Moore and Kleeman (1997) argued that variance growth in an ensemble prediction system for ENSO depends on the phase of the ENSO that initial condition comes from. It is shown that initial condition during the ENSO phase when the amplitude is high, the instability is reduced and the predictability becomes high. This explains the least error in the L5 predictability error. A Similar feature was observed with the previous version of the same model by DK10 also. It is interesting to note that L2 has the maximum predictability

Table 6 Seasonal (JJAS) forecast and predictability error at all the four study regions at different leads

Rain	ILR		EEIO		WEPO		EEPO	
	FE	PE	FE	PE	FE	PE	FE	PE
L5	3.89	0.50 (13 %)	3.02	0.65 (22 %)	3.19	0.82 (26 %)	1.75	0.47 (27 %)
L4	3.85	0.50 (13 %)	3.05	0.80 (26 %)	3.26	0.99 (30 %)	1.81	0.47 (26 %)
L3	3.90	0.56 (14 %)	3.11	0.83 (27 %)	3.45	1.07 (31 %)	1.84	0.49 (27 %)
L2	3.82	0.81 (21 %)	2.96	0.89 (30 %)	3.48	1.29 (37 %)	1.75	0.51 (29 %)
L1	3.58	0.78 (22 %)	2.99	1.00 (33 %)	3.23	1.07 (33 %)	1.70	0.46 (27 %)

The values in braces represents the percentage of predictability error (PE) with respect to the total error (i.e. forecast error-FE)
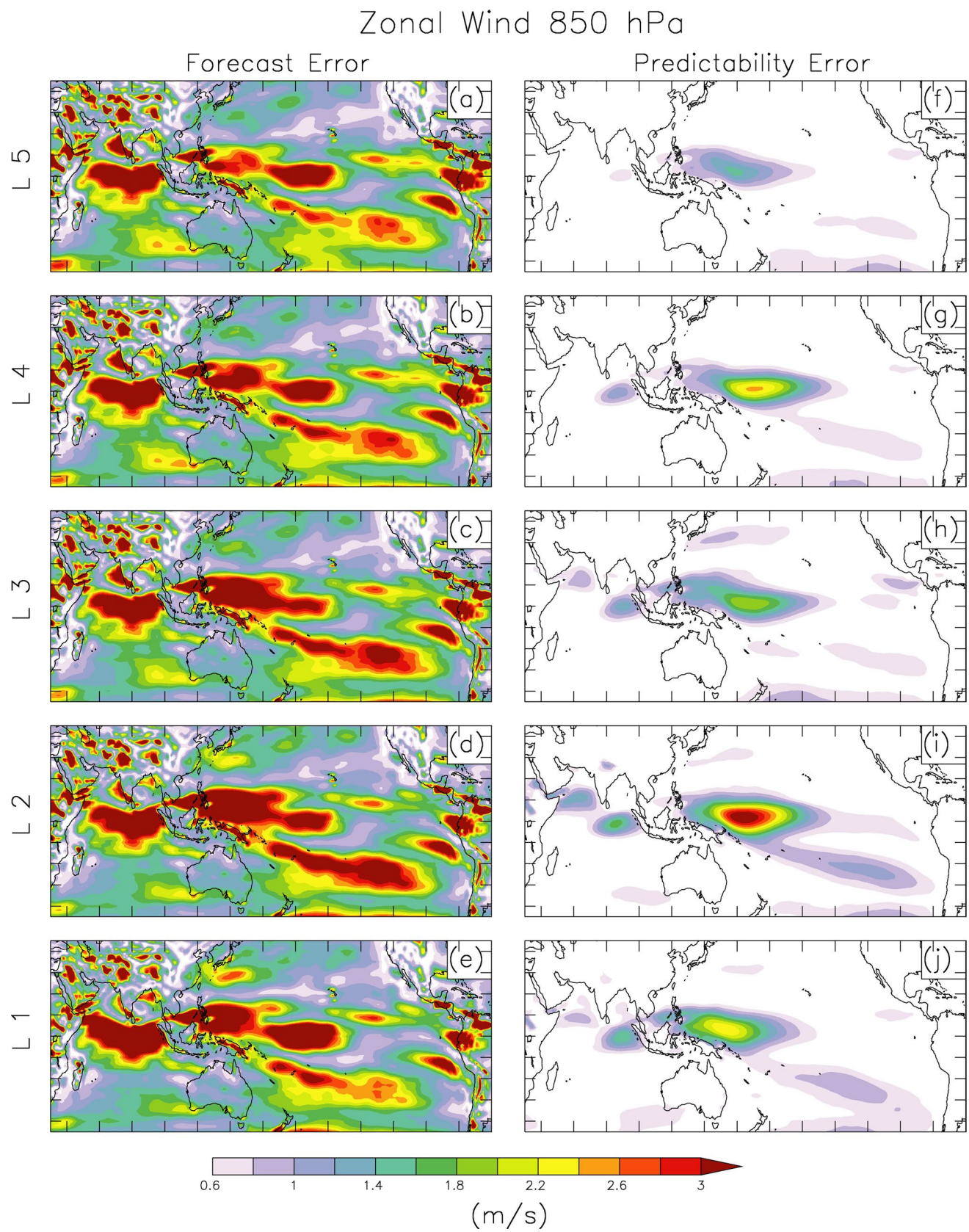
Zonal Wind 850 hPa

Forecast Error

Predictability Error

Fig. 9 Same as Fig. 8, but for 850 hPa Zonal wind

Table 7 Same as Table 6, but for zonal wind at 850 hPa for three oceanic regions

Wind 850	EEIO		WEPO		EEPO	
	FE	PE	FE	PE	FE	PE
L5	2.66	0.35 (13 %)	2.06	0.62 (30 %)	1.90	0.36 (19 %)
L4	2.72	0.50 (18 %)	2.18	0.86 (39 %)	1.91	0.38 (20 %)
L3	2.66	0.56 (21 %)	2.34	0.86 (37 %)	1.91	0.46 (24 %)
L2	2.78	0.74 (27 %)	2.54	1.14 (45 %)	1.76	0.47 (27 %)
L1	3.24	0.69 (21 %)	2.38	0.95 (40 %)	1.63	0.40 (25 %)

error concentrated over the equatorial western Pacific, including maritime continents, eastern equatorial Indian Ocean and also Indian land mass (typically over the central India and the foothills of Himalaya) and the Western Ghats of India. L2 (L1) represents most of the March (April) initial condition with some initial states coming from early April (May) month. The initialization during April–May is marked by the changing regimes of the mean winds (e.g. existence of westerly wind bursts in the region of prevailing easterlies over the equatorial Pacific Ocean), which may be some of the factors responsible for the predictability error if the model being initialized at this time. This error may be associated with the SPB effect of ENSO as discussed in the previous section.

The quantitative estimates of both forecast and predictability errors over the study region are given in Table 6. Forecast error is more or less constant over all the study region at all the leads as the range of error is marginal as compared to mean error. Furthermore the forecast error is highest over ILR (maximum error is 3.90 mm/day) and least over EEPO (maximum error is 1.84 mm/day). This clearly shows that the model simulates much better rainfall over the eastern Pacific region i.e. over the main spatial domain of ENSO dynamics and offers a great challenge for ISMR prediction. Predictability error, in general, has the greater contribution at L1 and L2, and least at L5 over all the study regions. WEPO (ILR) region has the largest (least) contribution of predictability error in terms of percentage contribution to the forecast error, which is 26–37 % (13–22 %). Thus, it is clear that one-third of the total error in rainfall (ISMR) may be contributed by the initial condition error, which is a significant portion of the total error.

6.2 Zonal wind 850 hPa

Most of the forecast error is concentrated over the equatorial zone and the most prominent being along the Indian Ocean basin and the western Pacific basin (Fig. 9a–e). Over the Southern Ocean of the Pacific basin and along the Western Ghats region of India, there exists a significant amount of the model forecast error. The forecast error over the Western Ghats (equatorial West Pacific) region decreases (increases) as the lead decreases and the forecast

error over the southern Pacific Ocean first increases and peaks at L2 then further decreases. It seems that there is a large model deficiency in simulating the zonal component of wind over the equatorial Indian Ocean basin. The error over the equatorial Indian Ocean seems to be not sensitive to the initialization. Predictability error is mostly present over the equatorial western Pacific basin and it increases as the lead decreases and peaks at L2 then further decreases (Fig. 9f–j). The same holds true for the equatorial eastern Indian Ocean basin. This implies that at L2 greater amount of total model error depends on the initialization error at the equatorial western Pacific basin (Fig. 9i). This clearly indicates the model's inability to capture the sudden westerly bursts of the zonal wind component in the area of the dominant easterlies, which may be due to the spring predictability barrier (Webster and Yang 1992) in particular during March (L3) and April (L2) leads. This is clearly seen in the predictability error in rainfall, cloud (figure not shown) and SST, indicating the dynamical consistency in the model. Table 7 shows these errors over the three oceanic regions for the zonal wind at 850 hPa. Predictability error has the largest contribution in WEPO region as compared to EEIO and EEPO regions, and it reaches up to 45 % in L2. This implies that initialization, too, is a great error contributor over these specific regions. Furthermore EEPO has the least forecast error (range 1.63–1.91 m/s) as compared to both EEIO (range 2.66–3.24 m/s) and WEPO (range 2.06–2.54 m/s).

6.3 SST

Similar to precipitation and zonal wind patterns at 850 hPa, SST also has large forecast error as compared to the predictability error (Fig. 10a–j). Most of the errors are concentrated over the sub-tropics rather than the tropics, except very narrow strip over the central and the eastern equatorial Pacific basin and the western Arabian Sea (off Somalia coast). Surprisingly the tropical (sub-tropical) forecast error increases (decreases) as the lead decreases. This indicates that for the larger leads, the influence of subtropics may be more important and for the shorter leads, tropics may play the major role. Significant SST forecast error results from the improper surface energy budget due to the ill
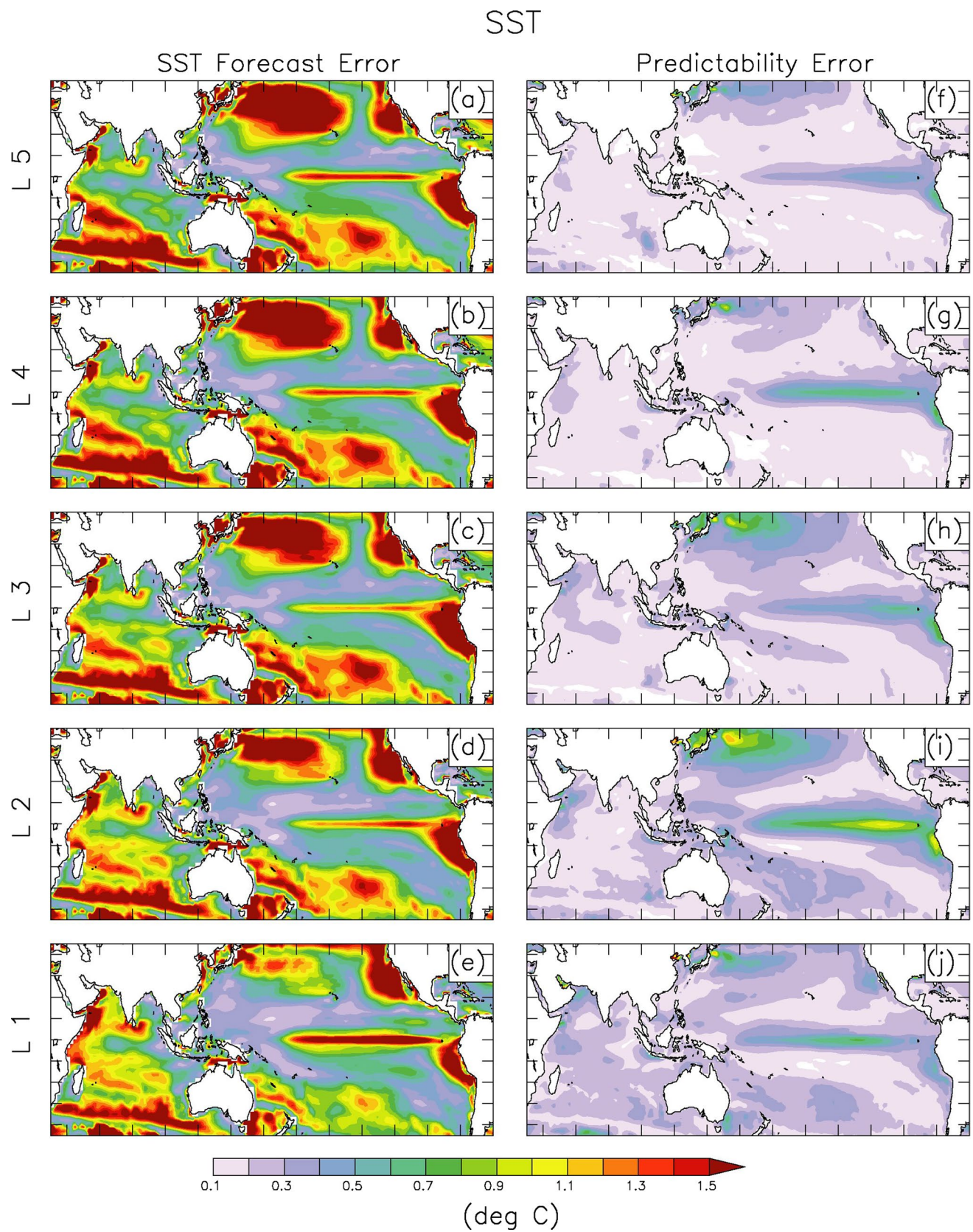
SST

Fig. 10 Same as Fig. 8, but for SST

Table 8 Same as Table 7, but for SST's

SST	EEIO		WEPO		EEPO	
	FE	PE	FE	PE	FE	PE
L5	0.72	0.14 (19 %)	0.61	0.16 (26 %)	0.85	0.27 (32 %)
L4	0.76	0.17 (22 %)	0.59	0.20 (34 %)	0.88	0.32 (36 %)
L3	0.80	0.20 (25 %)	0.57	0.22 (39 %)	0.95	0.32 (34 %)
L2	0.90	0.18 (20 %)	0.51	0.28 (55 %)	0.89	0.46 (52 %)
L1	0.94	0.24 (26 %)	0.52	0.23 (44 %)	0.86	0.28 (33 %)

representation of clouds (Zheng et al. 2011). The forecast error over the eastern Pacific basin near the Peru coast is solely due to under-representation of marine stratocumulus clouds (which reflects most of the shortwave radiation; e.g. Yoo et al. 2013). This is common to most of the coupled models of the present genre (Zheng et al. 2011). Ocean dynamics may also play some role due to less upwelling of cold water from beneath. For the rest of the region, over-estimation of model simulated low and middle level stratus/stratocumulus clouds may give rise to cold SST bias. The predictability errors are mainly confined over the east and central equatorial Pacific regions, north and northwest Pacific and Arabian Sea regions (Fig. 10f–j). In case of SST (Table 8), forecast error at WEPO (range 0.51–0.61 °C) is least as compared to EEIO (range 0.72–0.90 °C) and EEPO (range 0.85–0.95 °C). However, the percentage contribution of predictability error is maximum (range 26–55 %). Thus, WEPO region has the initialization error which is even larger than the model error at L2. Thus, accurate initial conditions have a greater role at some particular location and at particular lead as compared to model error.

7 Summary and conclusions

This study tries to explore the sensitivity of the initial conditions in terms of lead time for the seasonal retrospective forecast of rainfall and SST for the summer season (JJAS) in the NCEP CFSv2. The main focus of this study is to find out in detail the regions and factors responsible for ISMR predictability in terms of model errors and initial condition errors. In general predictability of ISMR is controlled by the Indian and the Pacific Ocean basins generated SST variability. Our study region consists of both these basins.

Model climatology in terms of seasonal mean and the inter-annual standard deviations are realistic and very close to that of the observed ones for rainfall, upper and lower level circulations and SST in all the leads, implying CFSv2 prediction is consistent at all the leads. Seasonal biases in precipitation, large-scale circulation at lower and upper levels and SST have a common tendency to decrease with the decrease in the forecast lead-time, clearly exhibiting the model drift. The dynamical consistency of biases

among all the variables augers well for the possibility of their rectification as these biases may be traced back to particular parameter(s) which may contribute to major part of the model error (Slingo and Palmer 2011). If we consider parameter wise bias, model simulated rainfall tends to be overestimated (underestimated) over oceanic (land) region. Overall rainfall tends to be more skillful at the least lead time (L0) as indicated by the large grid wise average correlation values at L0. However, bias in general does not follow the same trend. In case of the Indian land region, this correlation value is highest at L3 (0.21), despite having largest bias (−2.35 mm/day). L0 too has the same correlation (0.21) but with the least bias (−1.2 mm/day) over all the leads. Similarly, the bias of lower level wind at 850 hPa increases (decreases) as the lead decreases for the EEIO and WEPO (EEPO) regions. However, in the case of upper level winds at 200 hPa, the bias always decreases as the lead decreases over all the study regions. SST correlations constantly increase with the decreasing lead, but model cold SST bias seems to be pervasive and identical among all the leads with some regional exceptions. The region of the positive (negative) SST bias corresponds to the negative (positive) total cloud cover bias (figure not shown). This clearly hint at the role played by total cloud cover to significantly modulate the SSTs through the surface energy budget. Thus, the increase (decrease) in the bias with a decrease in lead in all parameters indicates that CFSv2 has best forecast skill at L0. However, the Indian subcontinent stands out as an exception.

The ISMR has maximum skill in L3, followed by L1 in all the independent data. These highest skill scores are 0.64, 0.42 and 0.57 with respect to GPCP, CMAP and IMD rainfall respectively for L3. However, two most important monsoon indices in terms of large-scale zonal wind shear (WY index) and SST over Niño3.4 region show maximum skill at L1 and L0 respectively. Further, there exists a strong spring predictability barrier of Niño3.4 and IOD index at L3. In spite of having better wind patterns, SST (according to WY, Niño3.4 index) in L1 and L0 and SPB in L3, ISMR prediction skill is maximum in L3. This maximization of ISMR skill at L3, despite significant ENSO SPB and better WY and Niño3.4 index at L1 and L0 adds one more dimension to the problem. Thus, predictability

of ISMR is perhaps controlled by the factors other than ENSO and IOD, which requires further detailed study. This is addressed in other manuscript in terms of both diagnostic and prognostic potential predictability using initial SST, snow and soil moisture conditions (Saha et al. 2015).

Furthermore, in CFSv2, most of the errors are contributed by the model imperfection and the initial conditions (as shown by the predictability error), has substantially less error. This is also common with the previous version of the model (DK10). Regions where forecast errors are high coincides with the regions having large negative/positive model bias. In general, forecast error tends to decrease with the decrease in the lead, except over a few regions. Model simulation at larger leads tends to have the least predictability error. The percentage contribution of the initial condition-based error to the model total error increases as the lead decreases and attain maximum value generally at L2. The SST predictability error is large over the eastern side of the equatorial Pacific basin and over the central north Pacific Ocean. Almost all the parameters show that the maximum predictability error occurs at L2 and over the equatorial western Pacific basin. This seems to be very important in the perspective of prediction of ISMR skill due to strong teleconnections. Similar to the bias, the predictability error of rainfall, zonal 850 hPa winds and SST are also dynamically consistent.

This study may be helpful in identifying the regions where model error and initial condition error may significantly affect the ISMR prediction. However, it has raised more queries and pave the way forward for detailed study on the reasons behind the L3 skill being maximum for the prediction of ISMR.

References

Adler RF, Huffman GJ, Chang A, Ferraro R, Xie P, Janowiak J, Rudolf B, Schneider U, Curtis S, Bolvin D, Gruber A, Susskind J, Arkin P, Nelkin E (2003) The version 2 Global Precipitation Climatology Project (GPCP) monthly precipitation analysis (1979–present). J Hydrometeorol 4:1147–1167

Ajaya Mohan RS, Goswami BN (2003) Potential predictability of the Asian summer monsoon on monthly and seasonal time scales. Atmos Phys, Meteor. doi:10.1007/s00703-002-0576-4

Ashok K, Zhaoyong G, Yamagata T (2001) Impact of the Indian Ocean dipole on the relationship between the Indian monsoon rainfall and ENSO. Res Lett, Geo. doi:10.1029/2001GL013294

Blanford HF (1884) On the connection of the Himalaya snow fall with dry winds and seasons of drought in India. Proc R Soc Lond 37:3–22

Brankovic C, Palmer TN, Ferranti L (1994) Predictability of seasonal atmospheric variations. J Clim 7:217–237

Charney JG, Shukla J (1981) Predictability of monsoons. In: Sir James Lighthill, Pearce (eds) Monsoon dynamics. Cambridge University Press, Cambridge, pp 99–109

Chaudhari HS, Pokhrel S, Mohanty S, Saha SK (2013a) Seasonal prediction of Indian summer monsoon in NCEP coupled and uncoupled model. Theor Appl Climatol 114:459–477

Chaudhari HS, Pokhrel S, Saha SK, Dhakate A, Yadav RK, Salunke K, Mahapatra S, Sabeerali CT, Rao SA (2013b) Model biases in long coupled runs of NCEP CFS in the context of Indian summer monsoon. Int J Climatol 33:1057–1069. doi:10.1002/joc.3489

Chen D, Zebiak SE, Busalacchi AJ, Cane MA (1995) An improved procedure for El Niño forecasting: implications for predictability. Science 269:1699–1702

Chen M, Wang W, Kumar A (2010) Prediction of monthly-mean temperature: the roles of atmospheric and land initial conditions and sea surface temperature. J Clim 23:717–725. doi:10.1175/2009JCLI3090.1

Clough SA, Shephard MW, Mlawer EJ, Delamere JS, Iacono MJ, Cady-Pereira K, Boukabara S, Brown PD (2005) Atmospheric radiative transfer modeling: a summary of the AER codes. J Quant Spectrosc Radiat Transf 91:233–244

Delsole T, Shukla J (2010) Model fidelity versus skill in seasonal forecasting. J Clim 23:4794–4806

Dirmeyer PA, Randal DK, Zhichang G (2006) Do global models properly represent the feedback between land and atmosphere? J Hydrometeorol 7:1177–1198

Drbohlav HKL, Krishnamurthy V (2010) Spatial structure, forecast errors, and predictability of the South Asian monsoon in CFS monthly retrospective forecasts. J Clim 23:4750–4769

Duan W, Wei C (2013) The 'spring predictability barrier' for ENSO predictions and its possible mechanism: results from a fully coupled model. Int J Climatol 33:1280–1292. doi:10.1002/joc.3513

Ek MB, Mitchell KE, Lin Y, Rogers E, Grunmann P, Koren V, Gayno G, Tarplay JD (2003) Implementation of Noah land surface model advances in the National Centers for Environmental Prediction operational mesoscale Eta model. J Geophys Res 1089(D22):8851. doi:10.1029/2002JD003296

Flohn H (1968) Contributions to a meteorology of the Tibetan Highlands. Rept. no. 130, Colorado State University, Fort Collins

Gadgil S, Rajeevan M, Nanjundiah R (2005) Monsoon prediction—why yet another failure? Curr Sci 88:1389–1400

Goswami BN (1998) Interannual variations of Indian summer monsoon in a GCM: external conditions versus internal feedbacks. J Clim 11:501–522

Goswami BN, Xavier PK (2003) Potential predictability and extended range prediction of Indian summer monsoon breaks. Geophys Res Lett 30(18):1966. doi:10.1029/2003GL017,810

Goswami BN, Krishnamurthy V, Aamalai H (1999) A broad-scale circulation index for the interannual variability of the Indian summer monsoon. Q J R Meteorol Soc 125:611–633

Goswami BN, Ajaya Mohan RS, Xavier PK, Sengupta D (2003) Clustering of low pressure systems during the Indian summer monsoon by intraseasonal oscillations. Geophys Res Lett 30(8):1431. doi:10.1029/2002GL01673

Griffies SM, Harrison MJ, Pacanowski RC, Rosati A (2004) A technical guide to MOM4. GFDL Ocean Group technical report 5, 337, GFDL

Hong S-Y, Pan H-L (1998) Convective trigger function for a mass-flux cumulus parameterization scheme. Mon Weather Rev 126:2599–2620

Iacono MJ, Mlawer EJ, Clough SA, Morcrette JJ (2000) Impact of an improved longwave radiation model, RRTM, on the energy budget and thermodynamic properties of the NCAR community climate model, CCM3. J Geophys Res 105:14873–14890

Kanamitsu M, Ebisuzaki W, Woollen J, Yang SK, Hnilo JJ, Fiorino M, Potter GL (2002) NCEP–DOE AMIP-II reanalysis (R-2). Bull Am Meteorol Soc 83:1631–1643

Kang IS, Shukla J (2005) Dynamical seasonal prediction and predictability of monsoon. In: Wang B (ed) The Asian monsoon. Praxis, Chichester

Kang IS, Lee JY, Park CK (2004) Potential predictability of summer mean precipitation in a dynamical seasonal prediction system with systematic error correction. J Clim 17(4):834–844

Kleeman R (2002) Measuring dynamical prediction utility using relative entropy. J Atmos Sci 59:2057–2072

Krishnamurthy V, Shukla J (2011) Predictability of the Indian monsoon in coupled general circulation models. COLA technical report 313

Krishnamurthy V, Shukla J (2012) Predictability of the Indian monsoon in coupled general circulation models. In: Tyagi A et al (eds) Monsoon monographs editor, vol II, chap 7. India Meteorological Department, New Delhi, pp 266–306

Krishnamurti TN, Bhalme HN (1976) Oscillations of monsoon system. Part I. Observational aspect. J Atmos Sci 33:1937–1954

Krishnamurti TN, Kanamitsu M, Kiss WJ, Lee JD, Krueger AF, Winston JS (1973) Tropical east–west circulations during the northern winter. J Atoms Sci 30:780–787

Kumar A, Hoerling MP (1998) Specification of regional sea surface temperatures in atmospheric general circulation model simulations. J Geophys Res 103:8901–8907

Lorenz EN (1963) Deterministic nonperiodic flow. J Atmos Sci 20:130–141

Moore AM, Kleeman R (1997) The singular vectors of a coupled ocean-atmosphere model of ENSO, Part I: Thermodynamics, energetics and error growth. Q J R Meteorol Soc 123:953–981

Naidu CV, Krishna KM, Rao SR, Kumar OSRUB, Durgalakshmi K, Ramakrishna SSVS (2011) Variations of Indian summer monsoon rainfall induce the weakening of easterly jet stream in the warming environment? Glob Planet Change 33:1017–1032

Parthasarathy B, Munot AA, Kothawale DR (1995) All India monthly and seasonal rainfall series: 1871–1993. Theor Appl Climatol 49:217–224

Phelps MW, Kumar A, O'Brien JJ (2004) Potential predictability in the NCEP CPC dynamical seasonal forecast system. J Clim 17:3775–3785

Pokhrel S, Chaudhari HS, Saha SK, Dhakate A, Yadav RK, Salunke K, Mahapatra S, Rao SA (2012a) ENSO, IOD and Indian summer monsoon in NCEP Climate Forecast System. Clim Dyn 39:2143–2165. doi:10.1007/s00382-012-1349-5

Pokhrel S, Rahaman H, Parekh A, Saha SK, Dhakate A, Chaudhari HS, Gairola RM (2012b) Evaporation-precipitation variability over Indian Ocean and its assessment in NCEP Climate Forecast System (CFSv2). Clim Dyn 39:2585–2608

Pokhrel S, Dhakate A, Chaudhari HS, Saha SK (2013) Status of NCEP CFS vis-a-vis IPCC AR4 models for the simulation of Indian summer monsoon. Theor Appl Climatol 111:65–78

Preethi B, Kripalani RH, Krishna Kumar K (2010) Indian summer monsoon rainfall variability in global coupled ocean-atmospheric models. Clim Dyn 35:1521–1539

Raghavan K (1973) Tibetan anticyclone and tropical easterly jet. Pure Appl Geophys PAGEOPH 110:2130–2142

Rajeevan M, Nanjundiah RS (2009) Coupled model simulations of twentieth century climate of the Indian summer monsoon. Curr Sci (Platinum jubilee special) 537–567

Rajeevan M, Pai DS, Anil Kumar R, Lal B (2006a) New statistical models for long-range forecasting of southwest monsoon rainfall over India. Clim Dyn. doi:10.1007/s00382-006-019706

Rajeevan M, Bhate J, Kale JD, Lal B (2006b) High resolution daily gridded rainfall data for the Indian region: analysis of break and active monsoon spells. Curr Sci 91:296–306

Rajeevan M, Unnikrishnan CK, Preethi B (2012) Evaluation of the ENSEMBLES multi-model seasonal forecasts of Indian summer monsoon variability. Clim Dyn 38:2257–2274

Rasmusson EM, Carpenter TH (1983) The relationship between eastern equatorial Pacific sea surface temperature and rainfall over India and Sri Lanka. Mon Weather Rev 111:517–528

Reichler T, Roads J (2005) Long range predictability in the tropics. Part II: 30–60 day variability. J Clim 18:634–650

Reynolds RW, Rayner NA, Smith TM, Stokes DC, Wang W (2002) An improved in situ and satellite SST analysis for climate. J Clim 15:1609–1625

Saha K (1970) Zonal anomaly of sea surface temperature in equatorial Indian Ocean and its possible effect upon monsoon circulation. Tellus 22(4):403–409

Saha S, Moorthi S, Pan H-L, Wu X, Wang J, Nadiga S, Tripp P, Kistler R, Woollen J, Behringer D, Liu H, Stokes D, Grumbine R, Gayno G, Wang J, Hou YT, Chuang HY, Juang H-MH, Sela J, Iredell M, Treadon R, Kleist D, Delst PV, Keyser D, Derber J, Ek M, Meng J, Wei H, Yang R, Lord S, Dool HVD, Kumar A, Wang W, Long C, Chelliah M, Xue Y, Huang B, Schemm JK, Ebisuzaki W, Lin R, Xie P, Chen M, Zhou S, Higgins W, Zou CZ, Liu Q, Chen Y, Han Y, Cucurull L, Reynolds RW, Rutledge G, Goldberg M (2010) The NCEP Climate Forecast System reanalysis. Bull Am Meteorol Soc 91:1015–1057

Saha SK, Halder S, Krishna Kumar K, Goswami BN (2011) Pre-onset land surface processes and internal interannual variabilities of the Indian summer monsoon. Clim Dyn 36:2077–2089

Saha SK, Halder S, Suryachandra A, Goswami BN (2012) Modulation of ISOs by land-atmosphere feedback and contribution to the interannual variability of Indian summer monsoon. J Geophys Res 117(D13101):1–14. doi:10.1029/2011JD017291

Saha SK, Pokhrel S, Chaudhari HS (2013) Influence of Eurasian snow on Indian summer monsoon in NCEP CFSv2 free run. Clim Dyn 41:1801–1815. doi:10.1007/s00382-012-1617-4

Saha S, Moorthi S, Wu X, Wang J, Nadiga S, Tripp P, Behringer D, Hou Y-T, Chuang H-Y, Iredell M, Ek M, Meng J, Yang R, Mendez M, van den Dool H, Zhang Q, Wang W, Chen M, Becker E (2014a) The NCEP Climate Forecast System version 2. J Clim 27:2185–2208. doi:10.1175/JCLI-D-12-00823.1

Saha SK, Pokhrel S, Chaudhari HS, Dhakate A, Shewale S, Sabeerali CT, Salunke K, Hazra A, Mahaptra S, Rao AS (2014b) Improved simulation of Indian summer monsoon in latest NCEP Climate Forecast System free run. Int J Climatol 34:1628–1641. doi:10.1002/joc.3791

Saha SK, Pokhrel S, Salunke K, Dhakate A, Chaudhari HS, Rahaman H, Krishna S, Hazra A, Sikka DR (2015) Potential predictability of Indian summer monsoon rainfall in NCEP CFSv2. J Adv Model Earth Syst (under review)

Sahai AK, Sharmila S, Abhilash S, Chattopadhyay R, Borah N, Krishna RPM, Joseph S, Roxy M, De S, Pattnaik S, Pillai P (2013) Simulation and extended range prediction of monsoon intraseasonal oscillations in NCEP CFS/GFS version 2 framework. Curr Sci 104(10):1394–1408

Samelson RG, Tziperman E (2001) Instability of the chaotic ENSO: the growth-phase predictability barrier. Journal of Atmospheric Sciences 58:3613–3625

Schott FA, Xie SP, McCreary JP (2009) Indian Ocean circulation and climate variability. Rev Geophys 47:1–46

Seo KH, Schemm JKE, Wang W, Kumar A (2007) The boreal summer intraseasonal oscillation simulated in the NCEP Climate Forecast System: the effect of sea surface temperature. Mon Weather Rev 135:1807–1827

Shinoda T, Hendon HH, Alexander MA (2004) Surface and subsurface dipole variability in the Indian Ocean and its relation with ENSO. Deep-Sea Res 51:619–635

Shukla J (1975) Effect of Arabian Sea-surface temperature anomaly on Indian Summer monsoon: a numerical experiment with the GFDL model. J Atmos Sci 32:503–511

Shukla J (1987) Interannual variability of monsoons. In: Fein JS, Stephens PL (eds) Monsoons. Wiley, London, pp 399–464

Shukla J (1998) Predictability in the midst of chaos: a scientific basis for climate forecasting. Science 282:728–731

Shukla J, Wallace JM (1983) Numerical simulation of the atmospheric response to equatorial Pacific sea surface temperature anomalies. J Atmos Sci 40:1613–1630

Sikka DR (1980) Some aspects of the large-scale fluctuations of summer monsoon rainfall over India in relation to fluctuations in the planetary and regional scale circulation parameters. Proc Ind Acad Sci (Earth Planet Sci) 89:179–195

Singh A, Acharya N, Mohanty UC, Robertson AW, Mishra G (2012) On the predictability of Indian summer monsoon rainfall in general circulation model at different lead time. Dyn Atmos Oceans 58:108–127

Slingo J, Palmer TN (2011) Uncertainty in weather and climate prediction. Philos Trans R Soc A 369:4751–4767

Soman MK, Slingo J (1997) Sensitivity of the Asian summer monsoon to aspects of sea-surface-temperature anomalies in the tropical Pacific Ocean. Q J R Meteorol Soc 123:309–336

Sperber KR, Palmer TN (1996) Interannual tropical rainfall variability in general circulation model simulations associated with the Atmospheric Model Intercomparison Project. J Clim 9:2727–2750

Sun B, Wang H (2013) Larger variability, better predictability? Int J Climatol 33:2341–2351

Taylor KE (2001) Summarizing multiple aspects of model performance in a single diagram. J Geophys Res 106(D7):7183–7192

Turner AG, Inness PM, Slingo JM (2005) The role of the basic state in the ENSO–monsoon relationship and implications for predictability. Q J R Meteorol Soc 131:781–804

van den Dool HM, Peng P, Johansson A, Chelliah M, Shabbar A, Saha S (2006) Seasonal-to-decadal predictability and prediction of North American climate—the Atlantic influence. J Clim 19:6005–6024

Walker GT (1924) Correlation in seasonal variations of weather, IX, A further study of world weather. Mem Indian Meteorol Dept 24(9):275–332

Wang B, Ding Q, Fu X, Kang IS, Jin K, Shukla J, Doblas-Reyes F (2005) Fundamental challenge in simulation and prediction of summer monsoon rainfall. Geophys Res Lett 32:L15711. doi:10.1029/2005GL022734

Webster PJ (1995) The annual cycle and the predictability of the tropical coupled ocean–atmosphere system. Meteorol Atmos Phys 56:33–55

Webster PJ, Yang S (1992) Monsoon and ENSO: selectively interactive systems. Q J R Meteorol Soc 118:877–926

Winton M (2000) A reformulated three-layer sea ice model. J Atmos Ocean Technol 17:525–531

Wu X, Simmonds I, Budd WF (1997) Modeling of Antarctic sea ice in a general circulation model. J Clim 10:593–609

Xie P, Arkin PA (1997) Global precipitation: a 17-year monthly analysis based on gauge observations, satellite estimates, and numerical model outputs. Bull Amer Meteorol Soc 78:2539–2558

Xue Y, Cane MA, Zebiak SE, Blumenthal MB (1994) On the prediction of ENSO: a study with a low order Markov model. Tellus 46A:512–528

Yanai M, Wu GX (2005) Effects of the Tibetan Plateau. In: Wang B (ed) The Asian monsoon. Praxis, Chichester

Yoo H, Li Z, Yu-Tai H, Lord S, Weng F, Barker HW (2013) Diagnosis and testing of low-level cloud parameterizations for the NCEP/GFS model using satellite and ground-based measurements. Clim Dyn 41:1595–1613. doi:10.1007/s00382-013-1884-8

Zheng Y, Shinoda T, Lin J-L, Kiladis GN (2011) Sea surface temperature biases under the stratus cloud deck in the southeast Pacific Ocean in 19 IPCC AR4 coupled general circulation models. J Clim 24:4139–4164